

# Journal of Materials Chemistry A

Accepted Manuscript



This is an *Accepted Manuscript*, which has been through the Royal Society of Chemistry peer review process and has been accepted for publication.

*Accepted Manuscripts* are published online shortly after acceptance, before technical editing, formatting and proof reading. Using this free service, authors can make their results available to the community, in citable form, before we publish the edited article. We will replace this *Accepted Manuscript* with the edited and formatted *Advance Article* as soon as it is available.

You can find more information about *Accepted Manuscripts* in the [Information for Authors](#).

Please note that technical editing may introduce minor changes to the text and/or graphics, which may alter content. The journal's standard [Terms & Conditions](#) and the [Ethical guidelines](#) still apply. In no event shall the Royal Society of Chemistry be held responsible for any errors or omissions in this *Accepted Manuscript* or any consequences arising from the use of any information it contains.

# Dopant-Free Organic Hole Transport Material for Efficient Planar Heterojunction Perovskite Solar Cells

Yongsheng Liu,<sup>a,b</sup> Qi Chen,<sup>a,b</sup> Hsin-Sheng Duan,<sup>a,b</sup> Huanping Zhou,<sup>a,b</sup> Yang (Michael) Yang,<sup>a</sup> Huajun Chen,<sup>a</sup> Song Luo,<sup>a,b</sup> Tze-Bin Song,<sup>a,b</sup> Letian Dou,<sup>a,b</sup> Ziruo Hong<sup>a</sup> and Yang Yang\*<sup>a,b</sup>

<sup>a</sup>Department of Materials Science and Engineering, University of California, Los Angeles, California 90095, USA

<sup>b</sup>California NanoSystems Institute, University of California, Los Angeles, California 90095, USA

E-mail: [yangy@ucla.edu](mailto:yangy@ucla.edu)

Keywords: dopant-free, hole transport material, perovskite solar cells, charge transport, transient photocurrent

## Abstract

We demonstrate efficient planar perovskite solar cells using dopant-free donor-acceptor (D-A) conjugated small molecule as hole transport material. The photovoltaic cell reaches a power conversion efficiency (PCE) of 14.9 %, which is comparable or even better than that of the devices using traditional doped 2,2',7,7'-tetrakis(N,N'-di-p-methoxyphenylamine)-9,9'-spirobifluorene (spiro-OMeTAD) hole transport material under equivalent conditions. We ascribe the high performance to the excellent charge transporting properties of the D-A conjugated small molecule. Time-resolved photoluminescence (PL), transient photocurrent response, and impedance spectroscopy characterization indicate that this D-A conjugated small molecule plays a key role in hole collection and extraction in perovskite based photovoltaic devices. The dopant-free D-A small molecule hole transport material used here not only

improves the efficiency, but also facilitates the fabrication process and thus potentially reduces the fabrication cost of perovskite solar cells.

## Introduction

Photovoltaic technology is one of the most effective approaches to utilize solar energy, which directly converts sunlight into electricity. Presently, the majority of commercial solar cells are based on inorganic materials such as silicon.<sup>1</sup> However, the high cost and large energy consumption of raw materials and expensive fabrication processes of the solar cells hinder their wide applications. To produce low-cost and high efficiency solar cells, many new photovoltaic technologies are being developed,<sup>2-6</sup> which include perovskite based organic-inorganic hybrid solar cells. This new class of photovoltaic devices has the promise to compete with current commercialized inorganic solar cells as they feature both a low cost fabrication process as well as high efficiency.

Recently, hybrid metal halide perovskites-such as  $\text{CH}_3\text{NH}_3\text{PbI}_3$  and  $\text{CH}_3\text{NH}_3\text{PbI}_{3-x}\text{Cl}_x$  show high photovoltaic performance due to their direct band gap, large absorption coefficient and high charge carrier mobility as well as very low loss in charge recombination.<sup>7-12</sup> An early reported power conversion efficiency (PCE) of 3.8% in 2009 has been promoted to over 16%, as new materials and novel device protocol were developed in the past few years.<sup>8-11, 13-21</sup> Although perovskites are efficient light harvesting materials with bipolar transport properties, recent reports of hole transport layer (HTL) free  $\text{TiO}_2/\text{CH}_3\text{NH}_3\text{PbI}_3$  heterojunction solar cells have resulted in PCEs of 8% to 10.85%,<sup>22, 23</sup> which are still much lower than that of the devices with HTLs. It indicates the necessity of interface modification for effective hole extraction from the perovskite layer to the anode. Proper energy level alignment and good hole transport properties

should be guaranteed to minimize any loss in electrical potential and charge recombination. To date, some HTL materials have been demonstrated in high-performance hybrid solar cells, among which 2,2',7,7'-tetrakis(N,N'-di-p-methoxyphenylamine)-9,9'-spirobifluorene (spiro-OMeTAD) is the ubiquitous material used. Using spiro-OMeTAD as a HTL, PCE of over 15% have been reported.<sup>15, 16, 20, 21</sup>

Spiro-OMeTAD HTL based perovskite photovoltaic devices have achieved the highest PCEs so far.<sup>21</sup> However, a pristine spiro-OMeTAD film suffers from a low hole mobility of  $\sim 10^{-4}$  cm<sup>2</sup> V<sup>-1</sup>s<sup>-1</sup> and low conductivity of  $\sim 10^{-5}$  S cm<sup>-2</sup> (compare with  $10^{-3}$  S cm<sup>-1</sup> for a typical halide perovskite) due to its amorphous nature.<sup>24, 25</sup> Thus ionic additives or p-type dopants, such as lithium bis(trifluoromethylsulfonyl)-imide (Li-TFSI), are required for spiro-OMeTAD HTL to generate free carriers and to increase its conductivity.<sup>8, 13, 16</sup> However, this material still has several disadvantages such as: (1) material cost due to the necessity of a thick spiro-OMeTAD layer (typically  $\sim 300$  nm);<sup>16, 20, 21</sup> (2) degradation of perovskite active layer as spiro-OMeTAD HTL based devices requires exposure to ambient atmosphere for proper functioning;<sup>26, 27</sup> (3) complex fabrication due to spiro-OMeTAD doping process.<sup>28</sup>

Thus alternative hole transport materials should be developed to replace spiro-OMeTAD.<sup>29-39</sup> Recently, a doped low band gap polymer, PDPPDBTE, was incorporated as HTL by Park et al. and the devices showed a PCE of 9.2%.<sup>34</sup> Seok et al. introduced a doped polymer hole transport material, poly-(triarylamine) (PTAA), yielding a certified PCE of 17.9% very recently, making the PTAA the best polymer HTL so far.<sup>37</sup> In addition, several conjugated polymers, such as P3HT, PCPDTBT and PCDTBT and so on, can be used, in spite of inferior PCEs.<sup>29, 32</sup> In all the cases, doping process is necessary, indicating these materials cannot afford enough carrier mobility, and thus certain carriers concentration is required for efficient hole extraction from

perovskite film. These potential challenges for HTLs, including the high cost, low mobility, and requirement of doping, should be tackled in order for us to make further advancement of perovskite solar cells.

As discussed above, an dopant-free HTL is highly desirable, though there has been no report on excellent photovoltaic performance based on HTL materials with such properties. Donor-Acceptor (D-A) conjugated small molecules with planar structures, possess tunable optical and electrical properties, facile synthesis, low production cost, and versatile wet processing procedures. The strong intermolecular interaction makes strong crystallization in solid thin films, and enables high charge carrier mobility. Therefore D-A conjugated small molecules are appropriate choices as HTLs and have been widely used as active semiconductor materials in organic electronic devices. Conjugated D-A small molecules HTLs have planar structure without diphenylamine group, which is the component of spiro-OMeTAD, increase the crystallinity and improve the mobility and conductivity of the pristine film. Also these molecules have easily tunable HOMO (highest occupied molecular orbital) energy level to allow for proper alignment with the perovskite absorbers. Thus D-A conjugated small molecules HTLs, though few, have shown good performance for perovskite solar cells.<sup>40, 41</sup> However, the study and comparison of D-A conjugated small molecules and traditional spiro-OMeTAD HTLs' effect on the performance of perovskite solar cells has rarely been reported.<sup>42, 43</sup>

In this work, we introduced a D-A conjugated small molecule DOR3T-TBDT (Figure 1), which shown good performance as a donor material in organic solar cells,<sup>44</sup> as dopant-free HTL in organic-inorganic hybrid solar cells consisting of  $\text{CH}_3\text{NH}_3\text{PbI}_{3-x}\text{Cl}_x$  as the light harvester and  $\text{TiO}_2$  as the electron transport layer (ETL). The photovoltaic devices using doped or dopant-free spiro-OMeTAD HTLs were also fabricated and tested for comparison. The device structure is

ITO/TiO<sub>2</sub>/CH<sub>3</sub>NH<sub>3</sub>PbI<sub>3-x</sub>Cl<sub>x</sub>/HTL/MoO<sub>3</sub>/Ag. The optimized devices showed a PCE up to 14.9%, which is the highest reported value so far for perovskite solar cells using dopant-free HTL. The performance of the perovskite solar cells using dopant-free small molecule HTL is comparable even better than that of the devices using traditional doped spiro-OMeTAD HTL under equivalent conditions. Our results highlight the application promise of the organic-inorganic hybrid perovskites solar cells using D-A conjugated small molecules with planar structure as dopant-free HTL due to its good packing structures thus relatively high mobility and conductivity.

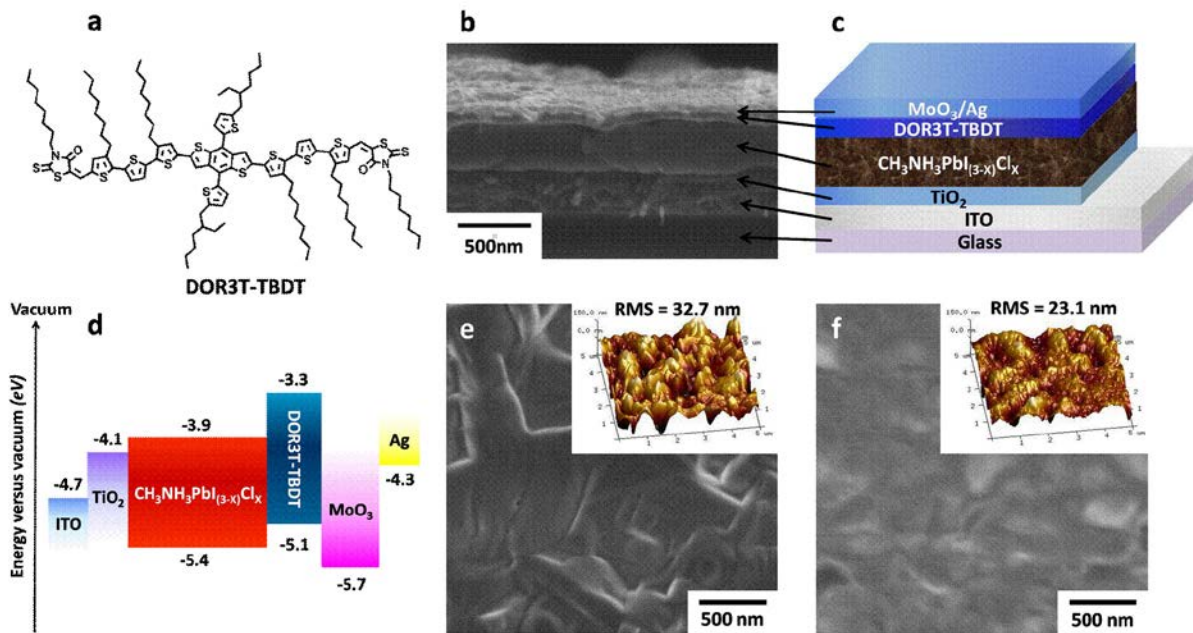


**Figure 1.** (a) Chemical structure of hole transport material DOR3T-TBDT. (b) SEM image of cross-sectional structure of the representative device. (c) Device structure of the solar cell. (d) Energy level diagram of the corresponding materials used in the device. (e) top-view SEM images of glass/TiO<sub>2</sub>/perovskite film; (f) top-view SEM images of glass/TiO<sub>2</sub>/perovskite/DOR3T-TBDT film. Insets are the tapping-mode AFM 3D topographic images of the related films.

## Results and discussion

The resistivity of DOR3T-TBDT was measured by transmission line model at room temperature, showing bulk conductivity of  $\sim 4 \times 10^{-4} \text{ S cm}^{-1}$ , which is comparable with those of lead halide perovskite ( $\sim 10^{-3} \text{ S cm}^{-1}$ ) and doped spiro-OMeTAD ( $\sim 10^{-4} \text{ S cm}^{-1}$ ).<sup>45</sup> High conductivity is expected to reduce the series resistance and improve the FF. The high conductivity is partially due to the high hole mobility. By using DOR3T-TBDT as a semiconductor layer in standard bottom-contact organic field-effect transistor (OFET), hole mobility of DOR3T-TBDT extracted from the linear regime was  $0.26 \text{ cm}^2 \text{ V}^{-1} \text{ s}^{-1}$ , which is three orders of magnitude larger than that of pristine spiro-OMeTAD ( $\sim 10^{-4} \text{ cm}^2 \text{ V}^{-1} \text{ s}^{-1}$ ).<sup>25</sup>

The cross-section SEM image and schematic of the device structure are shown in **Figure 1b** and **1c**. The overlayer of the small molecule HTL is seen to uniformly cap the perovskite layer. The cross-section SEM image of device confirms that the device configuration is a well-defined layer-by-layer structure. The thicknesses of the  $\text{TiO}_2$ ,  $\text{CH}_3\text{NH}_3\text{PbI}_{3-x}\text{Cl}_x$  and DOR3T-TBDT layers are  $\sim 40$ ,  $\sim 320$ , and  $\sim 60$  nm, respectively. Here, the  $\text{CH}_3\text{NH}_3\text{PbI}_{3-x}\text{Cl}_x$  layer is thick enough to serve as the light absorber and can effectively extract the charge carrier due to its long carrier diffusion lengths and good charge transport properties.<sup>46</sup> **Figure 1d** shows the relevant energy level diagram of the materials used to prepare the perovskite solar cells. In the case of  $\text{CH}_3\text{NH}_3\text{PbI}_{3-x}\text{Cl}_x$ , the valance band (VB) is  $\sim 5.4$  eV, which is measured from ultraviolet photoelectron spectroscopy (UPS).<sup>47</sup> Note that the HOMO level of DOR3T-TBDT is  $-5.5$  eV according to cyclic voltammetry (CV) measurement in its film state.<sup>44</sup> For comparison, we measured the HOMO level of DOR3T-TBDT and spiro-OMeTAD in film states using UPS (Figure S2, Supporting Information). The HOMO level of DOR3T-TBDT and spiro-OMeTAD are calculated to be  $-5.1$  and  $-5.0$  eV, respectively. The LUMO level of  $-3.3$  eV for DOR3T-TBDT was calculated from its optical band gap ( $1.77$  eV)<sup>42</sup> and HOMO level. As can be seen by

the band alignment,  $\text{CH}_3\text{NH}_3\text{PbI}_{3-x}\text{Cl}_x$  has a matched band position for heterojunction solar cells with  $\text{TiO}_2$  as ETL and DOR3T-TBDT as HTL.

The top-view scanning electron microscopy (SEM) images of the  $\text{CH}_3\text{NH}_3\text{PbI}_{3-x}\text{Cl}_x$  film on  $\text{TiO}_2$  and DOR3T-TBDT film on  $\text{CH}_3\text{NH}_3\text{PbI}_{3-x}\text{Cl}_x$  are shown in **Figure 1e** and **1f**. The results reveal that the perovskite film is uniform but exhibits relatively high roughness, though after coating small molecule HTL on the top of the perovskite layer, the surface appears smooth with complete coverage by HTL. The thin layer of DOR3T-TBDT efficiently prevents direct contact between the  $\text{CH}_3\text{NH}_3\text{PbI}_{3-x}\text{Cl}_x$  layer and the electrode, and at the same time plays a role in both hole extraction and transport. The surface morphology can also be seen from the tapping mode AFM images ( $5\ \mu\text{m} \times 5\ \mu\text{m}$ ) (insets of **Figure 1e** and **1f**). The roughness was reduced to 23.1 nm from 32.7 nm after spin coating a layer of DOR3T-TBDT on perovskite.

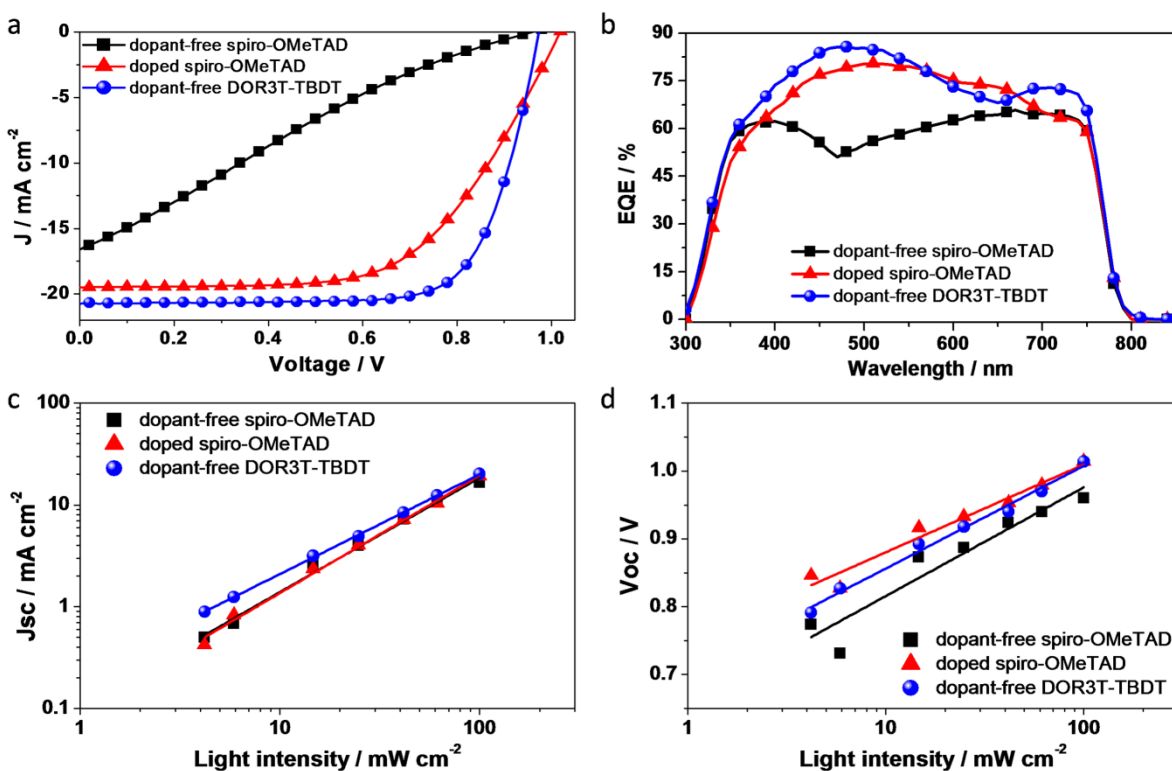


**Figure 2.** (a) Current density versus voltage (J–V) curves of perovskite solar cells using different HTLs under AM 1.5 G irradiation at  $100\ \text{mW cm}^{-2}$ . (b) EQE of the corresponding device using

different HTLs. (c)  $J_{SC}$  as a function of light intensity in a double-logarithmic scale for devices using different HTLs. (d)  $V_{OC}$  as a function of light intensity in a semi-logarithmic scale for devices using different HTLs.

To understand the effect of HTL on the performance of perovskite solar cells, various HTL materials including dopant-free small molecule DOR3T-TBDT, and dopant-free and doped spiro-OMETAD were used for comparison. **Figure 2a** shows the current density–voltage (J–V) curves of the optimized performance of three types of devices. As can be seen in the J–V curves and the summarized performance parameters in Table 1, the device with dopant-free spiro-OMETAD has a PCE of 3.5% with a low  $J_{SC}$  of  $16.6 \text{ mA cm}^{-2}$  and a poor FF of 22%. With reducing the incident light intensity to below  $10 \text{ mW cm}^{-2}$ , the FF increases to over 60% (Figure S7, Supporting Information). It indicates that the low hole mobility and conductivity of dopant-free spiro-OMETAD cause strong holes accumulation and the unusual J–V curve under AM1.5G 1 sun illumination. Using doped spiro-OMETAD HTL, we observed a dramatically enhanced performance with the highest PCE of 14.0%, combined with a  $J_{SC}$  of  $19.5 \text{ mA cm}^{-2}$ , an open circuit voltage ( $V_{OC}$ ) of 1.04 V, and an FF of 69.0%, mainly due to the improved conductivity of the spiro-OMETAD HTL, which is consistent with previously published results.<sup>46, 48</sup> Using DOR3T-TBDT as a HTL, the champion device exhibits a  $J_{SC}$  of  $20.7 \text{ mA cm}^{-2}$ , a  $V_{OC}$  of 0.97 V, and a very notable FF of 74%, yielding a PCE of 14.9%, which, to the best of our knowledge, is the highest PCE in planar heterojunction perovskite solar cells using an dopant-free HTL. The statistical data of perovskite solar cells containing dopant-free spiro-OMETAD, doped spiro-OMETAD and dopant-free DOR3T-TBDT HTLs are shown in Figure S9 (Supporting Information). It is worth noting that the dopant-free DOR3T-TBDT HTL facilitates very good charge injection under the forward bias, and thus yields a very low series resistance. However the doped spiro-OMETAD based device still exhibits higher resistance, which shall be

responsible for the lower FF and slightly higher  $V_{oc}$  than those of DOR3T-TBDT based devices. Indeed, the overall performance of the device using dopant-free DOR3T-TBDT HTL was comparable and even higher than that of the device using doped spiro-OMeTAD HTL. The high performance may stem from the matched HOMO energy level, high mobility and conductivity of this small molecule. We further doped DOR3T-TBDT with same dopants as in spiro-OMeTAD HTL, however, the device showed lower PCE ( $< 10\%$ ) (Figure S8, Supporting Information). Considering the doping efficiency, DOR3T-TBDT has a HOMO level of 5.1 eV, deeper than that of spiro-OMeTAD (5.0 eV). That means the dopants that work well with spiro-OMeTAD might not be able to generate free carriers in DOR3T-TBDT.<sup>49</sup> And also the dopants might play a negative role of disturbing the molecular packing. Nevertheless, p-type dopants with higher electron-affinity are expected to promote hole transport in the case of DOR3T-TBDT.

**Table 1.** Performance parameters for optimized photovoltaic devices prepared with different HTLs at reverse voltage scan.

HTLs	$V_{oc}$ (V)	$J_{sc}$ ( $\text{mA cm}^{-2}$ )	PCE (%)	FF (%)
Dopant-free spiro-OMeTAD	0.96	16.6	3.5	22
Doped spiro-OMeTAD	1.04	19.5	14.0	69
Dopant-free DOR3T-TBDT	0.97	20.7	14.9	74

From the J-V curve in **Figure 2**, the optimized device based on dopant-free small molecule HTL shows low serial resistance and good charge injection, resulting in a FF of 74%. The results indicate that this dopant-free small molecule HTL helps form ohmic contact between perovskite and anode for hole extraction and injection. Note that the film thickness of DOR3T-TBDT HTL

is ~60 nm, which is thinner than that (~300 nm) of doped spiro-OMeTAD HTL. The thin DOR3T-TBDT layer can potentially reduce material consumption for mass production. Our results indicate that comparable or even higher performance can be obtained for perovskite solar cells using dopant-free D-A small molecule with planar structure as HTL than that of dopant-free/doped spiro-OMeTAD HTLs (see Supporting Information, Figure S9, for statistical analysis). Note that MoO<sub>3</sub> used here formed a high work function contact buffer for efficient hole injection/extraction, and protected the underneath layers from damage caused by Ag deposition.<sup>50, 51</sup> **Figure 2b** shows the EQE spectra of the devices using different HTLs and J<sub>SC</sub> values calculated from the integral of EQE curves over AM1.5G solar spectrum are summarized in Table S1. The perovskite solar cells using DOR3T-TBDT as HTL show an excellent photocurrent response from 400 to 800 nm, with the EQE reaching a maximum of 86% at 480 nm, while dopant-free and doped spiro-OMeTAD based devices showed maximum EQE of 66% at 670 nm and 80% at 510 nm, respectively. The EQE values indicate that the photoresponse is very efficient for the device using DOR3T-TBDT HTL, which is slightly better than that of doped spiro-OMeTAD HTL.

In order to further understand losses due to the carrier recombination in the device, light intensity dependence of J-V characteristics of the device using different HTLs was measured under illumination of solar simulator with a set of neutral density filters. Shown in **Figure 2c** is the linear relation of photocurrent on light intensity in a double logarithmic scale for the device using dopant-free/doped spiro-OMeTAD and DOR3T-TBDT with a slope of very close to 1, indicating that the bimolecular recombination is very weak in these devices. **Figure 2d** gives V<sub>OC</sub> as a function of light intensity. We can see that V<sub>OC</sub> increases monotonically with light intensity for the perovskite solar cells using different HTLs. The dependence of V<sub>OC</sub> on light

intensity implies that trap-assisted Shockley-Read-Hall recombination plays a role.<sup>52</sup> We noticed that the slopes of Voc vs light intensity of the two high performance devices are still different. The doped spiro-OMeTAD based device has a smaller slope, which is tentatively ascribed to large shunt, since the thick HTL of 300 nm should be enough to ensure a large device shunt, and avoid any contact between perovskite photoactive layer and anode. On the other hand, the thickness of dopant-free DOR3T-TBDT layer is much smaller (~60 nm). Though it forms full coverage over the perovskite layer as shown in Fig. 1b, the shunt may still play a role reducing the Voc under weak light. Such recombination behaviors are consistent with FF vs light intensity as shown in Figure S7 (Supporting Information). The devices using dopant-free/doped spiro-OMeTAD showed low FF with increasing light intensity, suggesting charge recombination is dependent on photogenerated carrier density. On the contrary, the device using DOR3T-TBDT HTL showed high FF nearly constant under variable light intensity.

So far we show that hole extraction and transport are strongly dependent on the HTLs. To further look into the charge dynamics, we measured charge generation of the perovskite films via steady-state photoluminescence (PL) and time-resolved PL characterization. The steady-state PL spectra of glass/CH<sub>3</sub>NH<sub>3</sub>PbI<sub>3-x</sub>Cl<sub>x</sub>, glass/TiO<sub>2</sub>/CH<sub>3</sub>NH<sub>3</sub>PbI<sub>3-x</sub>Cl<sub>x</sub>, glass/CH<sub>3</sub>NH<sub>3</sub>PbI<sub>3-x</sub>Cl<sub>x</sub>/DOR3T-TBDT, and glass/TiO<sub>2</sub>/CH<sub>3</sub>NH<sub>3</sub>PbI<sub>3-x</sub>Cl<sub>x</sub>/DOR3T-TBDT are showed in **Figure 3a**. From the PL spectra, we observed a significant PL quenching when the perovskite layer is in contact with TiO<sub>2</sub> or DOR3T-TBDT layer, indicating efficient charge transfer at both interfaces.<sup>53,54</sup> Comparing with a perovskite film on glass substrate structure, the PL intensity is quenched to ~0.5% for perovskite layer coated on glass/TiO<sub>2</sub> substrate. The DOR3T-TBDT coated perovskite film shows almost completely quenched PL, and the sample exhibits roughly

0.2% PL, suggesting that this dopant-free DOR3T-TBDT HTL can extract charge carrier efficiently.

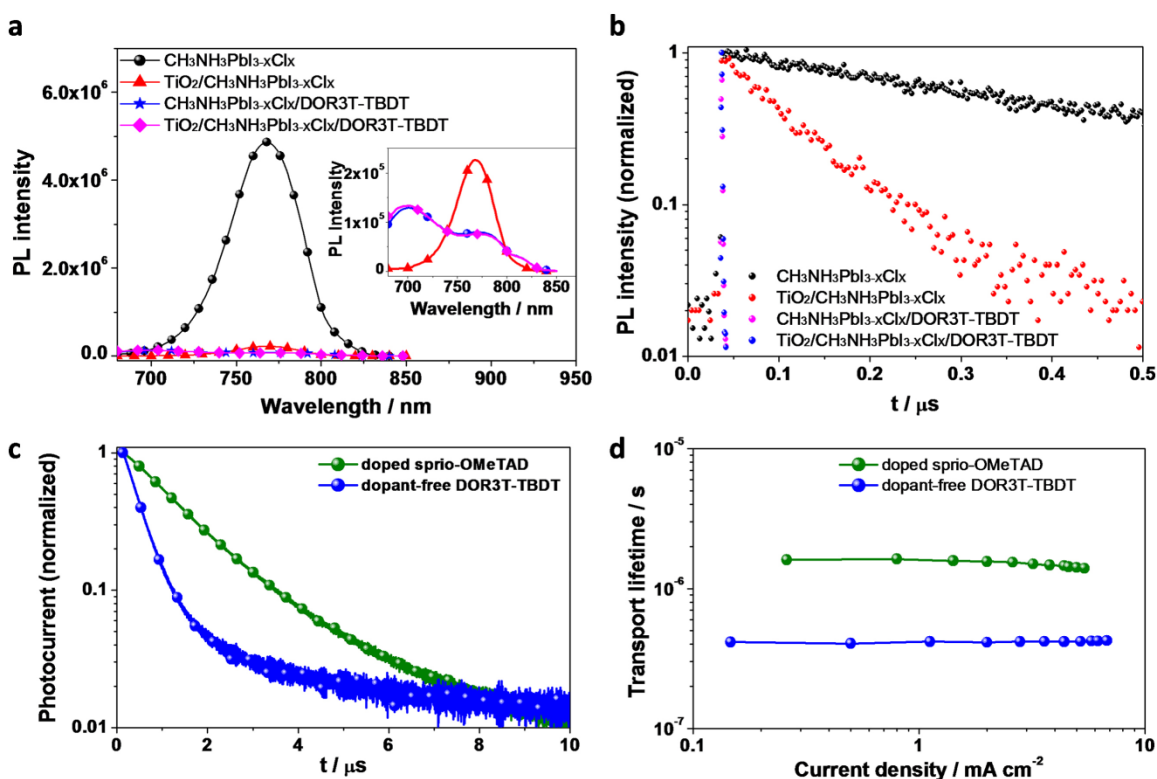


**Figure 3.** (a) The steady-state PL spectra and (b) Time-resolved PL decay transients spectra of glass/CH<sub>3</sub>NH<sub>3</sub>PbI<sub>3-x</sub>Cl<sub>x</sub>, glass/TiO<sub>2</sub>/CH<sub>3</sub>NH<sub>3</sub>PbI<sub>3-x</sub>Cl<sub>x</sub>, glass/CH<sub>3</sub>NH<sub>3</sub>PbI<sub>3-x</sub>Cl<sub>x</sub>/DOR3T-TBDT, and glass/TiO<sub>2</sub>/CH<sub>3</sub>NH<sub>3</sub>PbI<sub>3-x</sub>Cl<sub>x</sub>/DOR3T-TBDT. (c) Normalized photocurrent transients for perovskite solar cells with doped spiro-OMeTAD and dopant-free DOR3T-TBDT as HTL, set to the same background illumination intensity (50 mW cm<sup>-2</sup>). (d) Charge transport lifetime determined by small-perturbation transient photocurrent decay measurement of perovskite solar cells with doped spiro-OMeTAD and dopant-free DOR3T-TBDT as HTLs.

The time-resolved PL decay has been measured via monitoring the peak emission at 768 nm as shown in **Figure 3b**. Fitting the data with two-component exponential decay (here, the longer lifetime was used for comparison) yields the lifetime of carriers. The PL decay of the neat CH<sub>3</sub>NH<sub>3</sub>PbI<sub>3-x</sub>Cl<sub>x</sub> film exhibits a PL lifetime of 483 ns, which is larger than previous reports,<sup>46, 53</sup> and is tentatively ascribed to the Cl doping effect<sup>46</sup>. The PL lifetimes were substantially

shortened when perovskite was interfaced with the  $\text{TiO}_2$  layer with a PL lifetime 80 ns. As shown in **Figure 3b**, the decay of the perovskite/DOR3T-TBDT is significantly faster than that of  $\text{TiO}_2$ /perovskite. In addition, the PL lifetime cannot be monitored at the current temporal resolution, which indicates efficient charge-carrier transfer at the perovskite/DOR3T-TBDT interface.

To further investigate the dynamical processes operating under real device conditions, we measured carrier lifetimes by transient photocurrent measurements. As shown in **Figure 3c**, we observed that the DOR3T-TBDT devices exhibit faster transient photocurrent decays as compared to doped spiro-OMeTAD devices over various background light bias. **Figure 3d** displays the normalized photocurrent transients for DOR3T-TBDT based cells and for doped spiro-OMeTAD based cells, shows that the carrier collection in DOR3T-TBDT based cells is enhanced. Our results indicate that hole extraction has been improved by replacing doped Spiro-OMeTAD with DOR3T-TBDT.

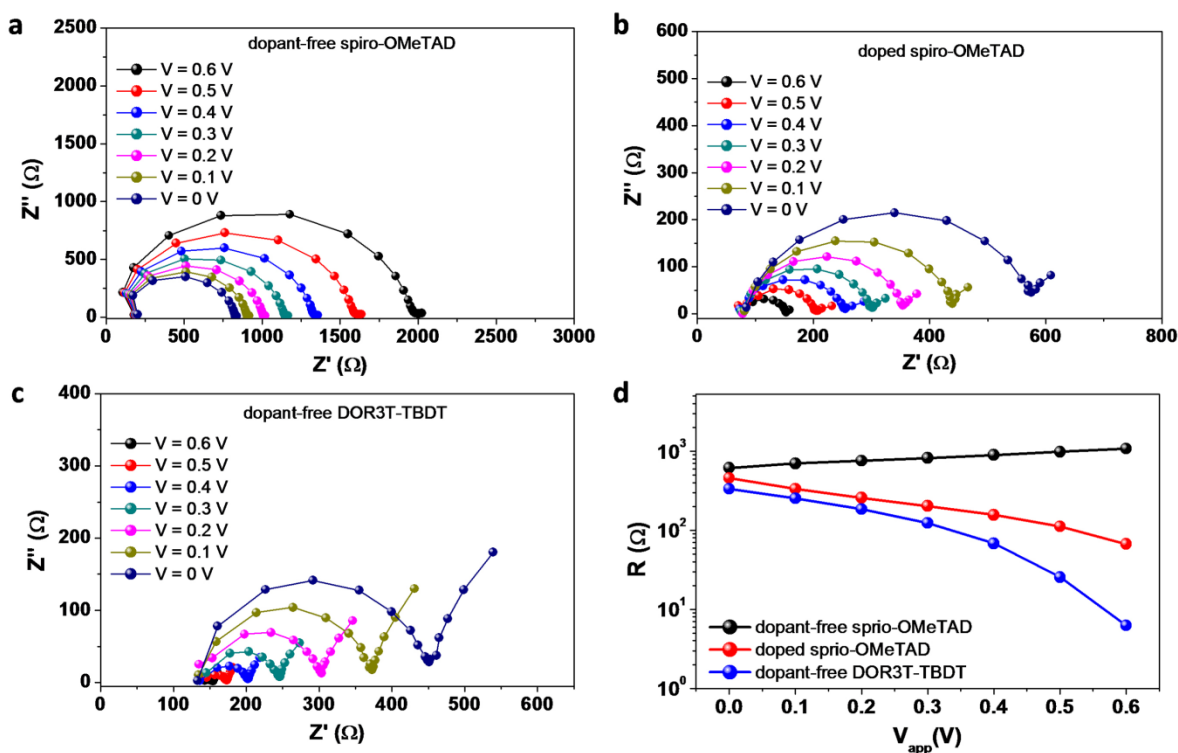


**Figure 4.** Bias dependence of Cole-Cole plots of device with (a) dopant-free spiro-OMeTAD HTL (b) doped spiro-OMeTAD HTL (c) dopant-free DOR3T-TBDT HTL. (d) Resistance extracted from impedance spectroscopy measurements at different potentials.

Again carrier recombination is still one of the major loss channels in photovoltaic cells. To gain more insight into the issue, electrochemical impedance spectroscopy (EIS) measurements were conducted on the completed devices under working conditions. Representative impedance spectra of perovskite devices using doped spiro-OMeTAD, dopant-free spiro-OMeTAD or DOR3T-TBDT as HTL were recorded at different applied voltage over the frequency range from 100 Hz to 1MHz under simulated AM1.5G 1 sun illumination ( $100 \text{ mW cm}^{-2}$ ). As shown in **Figure 4**, the Nyquist plots of these devices show two distinct features: (1) One main arc is observed for all the devices over the frequency range in the measurement; (2) a second arc can be partially seen in the spectra of the doped spiro-OMeTAD and DOR3T-TBDT cells. The absence of transmission line behavior, which is usually associated with significant tail states of  $\text{TiO}_2$ , is likely due to the very thin  $\text{TiO}_2$  layer employed in the devices.<sup>30</sup> For mesoporous  $\text{TiO}_2$  based solid state dye sensitized solar cells, the high frequency features represent the hole transport properties.<sup>55-57</sup> In addition, since the active layer and ETL conditions are kept the same, the different diameters (resistance) shall be related to the carrier transport and contact-resistance in various HTL layers. Thus, we fitted the spectra with a resistance in series of a high frequency parallel RC circuit, so as to extract the information regarding hole transport and extraction. We exclude the low frequency features in the fitting, considering that the electron transport is not in the scope of this study. The fitting results are summarized in **Figure 4d**, showing the dependence of hole transport resistance on applied voltages. The hole transport resistance decreases with increasing potential for both DOR3T-TBDT and doped spiro-OMeTAD based devices, and the resistance value for DOR3T-TBDT based device decreases more dramatically than that of doped

spiro-OMeTAD, indicating the smoother carrier movement as a result of reduced resistive losses. This is consistent with its enhanced FF. In contrast, the device using dopant-free spiro-OMeTAD HTL exhibits severe charge accumulation due to poor hole conductivity in the HTL, and the behavior of the solar cell resembles that of a huge resistor or injection barrier due to the lack of the doping ions in spiro-OMeTAD. It might be a concern that the absorption of HTL overlaps with that of perovskite photoactive layer, and reduces photovoltaic efficiency. We argue that the photogenerated excitons can still be converted into free carriers and collected with proper device design.<sup>58</sup> Note that the representative perovskite/DOR3T-TBDT based device shows hysteresis in the J–V curves (Figure S10, Supporting Information), which is similar to those seen in typical perovskite devices.<sup>21, 59-61</sup> The detailed data are shown in Table S2 (Supporting Information).

## Conclusions

In conclusion, we have successfully demonstrated efficient planar structure perovskite solar cells employing a dopant-free small molecule HTL. The optimized device exhibits an impressive PCE of 14.9%, which is comparable even better than that of the devices using traditional doped spiro-OMeTAD hole transport layer under equivalent conditions, and thus highlights the potential of dopant-free small molecule HTL for high performance perovskite solar cells. Time-resolved photoluminescence (PL), transient photocurrent, and impedance spectra characterization indicate that this D-A conjugated small molecule can efficiently extract holes from the perovskite film to the anode. Our device legitimizes the use of D-A small molecules as HTLs in perovskite based solar cells as our small molecule HTL improves the efficiency, facilitates the fabrication process and reduces the fabrication cost. Our results indicate that D-A conjugated small molecules, which have good packing structure thus relatively high mobility and conductivity, are a class of promising hole transporting materials, thus broader organic molecular semiconductors can be

applied to the perovskite solar cells. The use of dopant-free D-A conjugated small molecule HTLs will greatly enhance the potential for commercial applications of perovskite solar cells and thus can compete with the traditional inorganic solar cells.

## Experimental Section

*Solar cell fabrication and measurement:* A 40-nm-thick layer of TiO<sub>2</sub> nanoparticle in ethanol with the appropriate amount of TiAcAc was spin-coated onto an ITO glass substrate and annealed at 150 °C for 30 min. Next, the substrates were transferred into a nitrogen-filled glove box. A solution of CH<sub>3</sub>NH<sub>3</sub>PbI<sub>3-x</sub>Cl<sub>x</sub> in DMF was then spin coated onto the ITO/TiO<sub>2</sub> substrate by spin-coating at 2000 rpm for 30 s. For the CH<sub>3</sub>NH<sub>3</sub>PbI<sub>3-x</sub>Cl<sub>x</sub> perovskite layer, the CH<sub>3</sub>NH<sub>3</sub>I powder was mixed with PbCl<sub>2</sub> at a 3:1 mol ratio in DMF at 60 °C for 12 h. Specifically, the concentration of the PbCl<sub>2</sub> and CH<sub>3</sub>NH<sub>3</sub>I were 0.7 and 2.1 M, respectively. The films were then dried on a hot plate at 95 °C for 90 min in air. The dopant-free DOR3T-TBDT HTL was spin-coated onto the perovskite layer. Here the concentration of DOR3T-TBDT is 18 mg ml<sup>-1</sup> in chloroform and the film thickness is ~60 nm. The doped DOR3T-TBDT/chloroform (18 mg/ml, 0.4ml) solution was prepared with addition of 3 μL Li-TFSI/acetonitrile (260 mg/mL), and 5 μL tert-butylpyridine (tBP). The doped or dopant-free spiro-OMeTAD HTL was coated by spin coating (2,000 r.p.m. for 30 s) 25 μl of chlorobenzene solution. The spiro-OMeTAD without dopant has the concentration of 160 mg/ml. For a doped solution, a spiro-OMeTAD/chlorobenzene (160 mg/1 mL) solution was employed with addition of 35 μL Li-TFSI/acetonitrile (260 mg/mL), and 28 μL 4-tert-Butylpyridine. Finally, a 15 nm MoO<sub>3</sub> layer and a 150 nm Ag layer were deposited in sequence on the HTL through shadow masks via thermal evaporation under high vacuum (~2×10<sup>-6</sup> Torr). The effective area was 0.1 cm<sup>2</sup>. The current density-voltage (J-V) characteristics of photovoltaic devices were obtained by a Keithley

2400 source-measure unit. The photocurrent was measured under AM 1.5 G illumination at 100 mW cm<sup>-2</sup> under a Newport Thermal Oriel 91192 1000 W solar simulator. Unless stated otherwise, the devices were masked and measured under the reverse voltage scan with a scan rate of 1 V s<sup>-1</sup>. The light intensity was calibrated by KG-5 Si diode. External quantum efficiencies were measured by an Enli Technology (Taiwan) EQE measurement system. The effective area of each cell was 0.1 cm<sup>2</sup> defined by masks for all the photovoltaic devices discussed in this work.

*Transient photocurrent decay measurements:* A white light bias was generated from an array of diodes (Molex 180081-4320) to simulate 1 sun working condition. A pulsed red dye laser (Rhodamine 6G, 590nm) pumped by a nitrogen laser (LSI VSL-337ND-S) was used as the perturbation source, with a pulse width of 4 ns and a repetition frequency of 10 Hz. The perturbation light intensity was attenuated to keep the amplitude of transient  $\Delta V$  below 5 mV. The current dynamics were recorded on a digital oscilloscope (Tektronix DPO 4104B), and the currents at short circuit condition were measured over a 50 $\Omega$  resistor.

*Impedance spectroscopy measurements:* The complex impedance of the devices was recorded over the frequency range from 100 Hz to 1 MHz at the room temperature under 1 sun, using the Z- $\theta$  mode of a HP 4284A LCR precision meter. An AC drive bias of 30 mV and different DC voltages range from 0 to 0.9 V with a step of 0.1 V was employed. The EIS Spectrum Analyzer was used for the fitting of the impedance spectra.

### **Acknowledgements**

The authors gratefully acknowledge the financial support from the Office of Naval Research (Grant No. N000141110250), National Science Foundation (Grant No. DMR-1335645), and the Enli Tech (in Taiwan) for donating the EQE measurement system to UCLA. The authors would

like to thank Dr. Jingbi You and Dr. Wan-Ching Hsu for helpful discussion and Mr. Eric Young and Mr. Nicholas De Marco for proof reading of this manuscript. The authors would lastly like to thank and acknowledge the use of the Nano and Pico Characterization Lab at the California NanoSystems Institute for AFM analysis.

**Electronic Supplementary Information (ESI) available:** ESI contains additional spectroscopic and J-V data, information about the organic field-effect transistors, XRD and AFM, and box chart of device parameters.

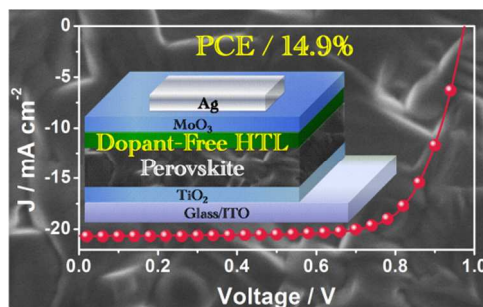
#### Reference List

1. T. Saga, *Npg. Asia Mater*, **2010**, *2*, 96-102.
2. M. A. Green, K. Emery, Y. Hishikawa, W. Warta and E. D. Dunlop, *Prog. Photovoltaics*, **2014**, *22*, 1-9.
3. G. Li, R. Zhu and Y. Yang, *Nat. Photonics*, **2012**, *6*, 153-161.
4. S. Mathew, A. Yella, P. Gao, R. Humphry-Baker, B. F. E. Curchod, N. Ashari-Astani, I. Tavernelli, U. Rothlisberger, M. K. Nazeeruddin and M. Gratzel, *Nat. Chem.* **2014**, *6*, 242-247.
5. R. F. Service, *Science*, **2013**, *342*, 794-797.
6. N. G. Park, *J Phys Chem Lett*, 2013, **4**, 2423-2429.
7. C. C. Stoumpos, C. D. Malliakas and M. G. Kanatzidis, *Inorg Chem*, **2013**, *52*, 9019-9038.
8. H. S. Kim, C. R. Lee, J. H. Im, K. B. Lee, T. Moehl, A. Marchioro, S. J. Moon, R. Humphry-Baker, J. H. Yum, J. E. Moser, M. Gratzel and N. G. Park, *Sci. Rep.* **2012**, *2*, 591.
9. P. Gao, M. Gratzel and M. K. Nazeeruddin, *Energ. Environ. Sci.* **2014**, *7*, 2448-2463.
10. M. A. Green, A. Ho-Baillie and H. J. Snaith, *Nat. Photonics*, **2014**, *8*, 506-514
11. A. Kojima, K. Teshima, Y. Shirai and T. Miyasaka, *J. Am. Chem. Soc.* 2009, **131**, 6050-6051.
12. M. Gratzel, *Nat. Mater.* **2014**, *13*, 838-842.
13. J. Burschka, N. Pellet, S. J. Moon, R. Humphry-Baker, P. Gao, M. K. Nazeeruddin and M. Gratzel, *Nature*, **2013**, *499*, 316-319.
14. Q. Chen, H. P. Zhou, Z. R. Hong, S. Luo, H. S. Duan, H. H. Wang, Y. S. Liu, G. Li and Y. Yang, *J. Am. Chem. Soc.* **2014**, *136*, 622-625.

15. M. M. Lee, J. Teuscher, T. Miyasaka, T. N. Murakami and H. J. Snaith, *Science*, **2012**, *338*, 643-647.
16. M. Z. Liu, M. B. Johnston and H. J. Snaith, *Nature*, **2013**, *501*, 395-398.
17. J. B. You, Z. R. Hong, Y. Yang, Q. Chen, M. Cai, T. B. Song, C. C. Chen, S. R. Lu, Y. S. Liu, H. P. Zhou and Y. Yang, *Acs Nano*, **2014**, *8*, 1674-1680.
18. N. J. Jeon, H. G. Lee, Y. C. Kim, J. Seo, J. H. Noh, J. Lee and S. I. Seok, *J. Am. Chem. Soc.* **2014**, *136*, 7837-7840.
19. N. J. Jeon, J. H. Noh, Y. C. Kim, W. S. Yang, S. Ryu and S. I. Seok, *Nat. Mater.* **2014**, *13*, 897-903.
20. J. W. Lee, D. J. Seo, A. N. Cho and N. G. Park, *Adv. Mater.* **2014**, *26*, 4991-4998.
21. H. P. Zhou, Q. Chen, G. Li, S. Luo, T. B. Song, H. S. Duan, Z. R. Hong, J. B. You, Y. S. Liu and Y. Yang, *Science*, **2014**, *345*, 542-546.
22. W. Abu Laban and L. Etgar, *Energ. Environ. Sci.* **2013**, *6*, 3249-3253.
23. S. Aharon, S. Gamliel, B. El Cohen and L. Etgar, *Phys. Chem. Chem. Phys.* **2014**, *16*, 10512-10518.
24. J. Burschka, A. Dualeh, F. Kessler, E. Baranoff, N. L. Cevey-Ha, C. Y. Yi, M. K. Nazeeruddin and M. Gratzel, *J. Am. Chem. Soc.* **2011**, *133*, 18042-18045.
25. T. Leijtens, I. K. Ding, T. Giovenzana, J. T. Bloking, M. D. McGehee and A. Sellinger, *Acs Nano* **2012**, *6*, 1455-1462.
26. A. Abate, T. Leijtens, S. Pathak, J. Teuscher, R. Avolio, M. E. Errico, J. Kirkpatrick, J. M. Ball, P. Docampo, I. McPherson and H. J. Snaith, *Phys. Chem. Chem. Phys.* **2013**, *15*, 2572-2579.
27. G. E. Eperon, V. M. Burlakov, P. Docampo, A. Goriely and H. J. Snaith, *Adv. Funct. Mater.* **2014**, *24*, 151-157.
28. J. Liu, Y. Z. Wu, C. J. Qin, X. D. Yang, T. Yasuda, A. Islam, K. Zhang, W. Q. Peng, W. Chen and L. Y. Han, *Energ. Environ. Sci.* **2014**, *7*, 2963-2967.
29. D. Q. Bi, L. Yang, G. Boschloo, A. Hagfeldt and E. M. J. Johansson, *J. Phys. Chem. Lett.* **2013**, *4*, 1532-1536.
30. J. A. Christians, R. C. M. Fung and P. V. Kamat, *J. Am. Chem. Soc.* **2014**, *136*, 758-764.
31. B. Conings, L. Baeten, C. D. Dobbelaere, J. D'Haen, J. Manca and H. G. Boyen, *Adv. Mater.* **2014**, *26*, 2041-2046.
32. J. H. Heo, S. H. Im, J. H. Noh, T. N. Mandal, C. S. Lim, J. A. Chang, Y. H. Lee, H. J. Kim, A. Sarkar, M. K. Nazeeruddin, M. Gratzel and S. I. Seok, *Nat. Photonics*, **2013**, *7*, 487-492.
33. A. Krishna, D. Sabba, H. R. Li, J. Yin, P. P. Boix, C. Soci, S. G. Mhaisalkar and A. C. Grimsdale, *Chem. Sci.* **2014**, *5*, 2702-2709.
34. Y. S. Kwon, J. Lim, H. J. Yun, Y. H. Kim and T. Park, *Energ. Environ. Sci.* **2014**, *7*, 1454-1460.
35. O. Malinkiewicz, A. Yella, Y. H. Lee, G. M. Espallargas, M. Graetzel, M. K. Nazeeruddin and H. J. Bolink, *Nat. Photonics*, **2014**, *8*, 128-132.
36. P. Qin, S. Tanaka, S. Ito, N. Tetreault, K. Manabe, H. Nishino, M. K. Nazeeruddin and M. Gratzel, *Nat. Commun.* **2014**, *5*, 3834/1-6.
37. N. J. Jeon, J. H. Noh, W. S. Yang, Y. C. Kim, S. C. Ryu, J. W. Seo and S. I. Seok, *Nature*, **2015**, *517*, 476-480.
38. S. Guarnera, A. Abate, W. Zhang, J. M. Foster, G. Richardson, A. Petrozza and H. J. Snaith, *J. Phys. Chem. Lett.* **2015**, *6*, 432-437.

39. Z. Hawash, L. K. Ono, S. R. Raga, M. V. Lee and Y. B. Qi, *Chem. Mater.* **2015**, *27*, 562-569.
40. P. Qin, S. Paek, M. I. Dar, N. Pellet, J. Ko, M. Gratzel and M. K. Nazeeruddin, *J. Am. Chem. Soc.* **2014**, *136*, 8516-8519.
41. P. Qin, H. Kast, M. K. Nazeeruddin, S. M. Zakeeruddin, A. Mishra, P. Bauerle and M. Gratzel, *Energ. Environ. Sci.* **2014**, *7*, 2981-2985.
42. M. Cheng, C. Chen, X. C. Yang, J. Huang, F. G. Zhang, B. Xu and L. C. Sun, *Chem. Mater.* **2015**, *27*, 1808-1814.
43. Y. K. Song, S. T. Lv, X. C. Liu, X. G. Li, S. R. Wang, H. Y. Wei, D. M. Li, Y. Xiao and Q. B. Meng, *Chem. Commun.* **2014**, *50*, 15239-15242.
44. Y. S. Liu, C. C. Chen, Z. R. Hong, J. Gao, Y. Yang, H. P. Zhou, L. T. Dou, G. Li and Y. Yang, *Sci. Rep.* **2013**, *3*, 3356/1-8.
45. T. Leijtens, J. Lim, J. Teuscher, T. Park and H. J. Snaith, *Adv. Mater.* **2013**, *25*, 3227-3233.
46. S. D. Stranks, G. E. Eperon, G. Grancini, C. Menelaou, M. J. P. Alcocer, T. Leijtens, L. M. Herz, A. Petrozza and H. J. Snaith, *Science*, **2013**, *342*, 341-344.
47. P. Schulz, E. Edri, S. Kirmayer, G. Hodes, D. Cahen and A. Kahn, *Energ. Environ. Sci.* **2014**, *7*, 1377-1381.
48. K. Wojciechowski, M. Saliba, T. Leijtens, A. Abate and H. J. Snaith, *Energ. Environ. Sci.* **2014**, *7*, 1142-1147.
49. K. Walzer, B. Maennig, M. Pfeiffer and K. Leo, *Chem. Rev.* **2007**, *107*, 1233-1271.
50. D. W. Zhao, P. Liu, X. W. Sun, S. T. Tan, L. Ke and A. K. K. Kyaw, *Appl. Phys. Lett.* **2009**, *95*, 153304/1-4.
51. T. Hori, T. Shibata, V. Kittichungchit, H. Moritou, J. Sakai, H. Kubo, A. Fujii and M. Ozaki, *Thin Solid Films*, **2009**, *518*, 522-525.
52. M. M. Mandoc, F. B. Kooistra, J. C. Hummelen, B. de Boer and P. W. M. Blom, *Appl. Phys. Lett.* **2007**, *91*, 263505/1-3.
53. G. C. Xing, N. Mathews, S. Y. Sun, S. S. Lim, Y. M. Lam, M. Gratzel, S. Mhaisalkar and T. C. Sum, *Science*, **2013**, *342*, 344-347.
54. H. Najafov, B. Lee, Q. Zhou, L. C. Feldman and V. Podzorov, *Nat. Mater.* **2010**, *9*, 938-943.
55. H. S. Kim, J. W. Lee, N. Yantara, P. P. Boix, S. A. Kulkarni, S. Mhaisalkar, M. Gratzel and N. G. Park, *Nano Lett.* **2013**, *13*, 2412-2417.
56. A. Dualeh, T. Moehl, N. Tetreault, J. Teuscher, P. Gao, M. K. Nazeeruddin and M. Gratzel, *Acs Nano* **2014**, *8*, 362-373.
57. H. S. Kim, I. Mora-Sero, V. Gonzalez-Pedro, F. Fabregat-Santiago, E. J. Juarez-Perez, N. G. Park and J. Bisquert, *Nat. Commun.* **2013**, *4*, 2242/1-7.
58. Y. S. Liu, Z. R. Hong, Q. Chen, W. H. Chang, H. P. Zhou, T. B. Song, E. Young, Y. Yang, J. B. You, G. Li and Y. Yang, *Nano Lett.* **2015**, *15*, 662-668.
59. H. J. Snaith, A. Abate, J. M. Ball, G. E. Eperon, T. Leijtens, N. K. Noel, S. D. Stranks, J. T. W. Wang, K. Wojciechowski and W. Zhang, *J. Phys. Chem. Lett.* **2014**, *5*, 1511-1515.
60. E. L. Unger, E. T. Hoke, C. D. Bailie, W. H. Nguyen, A. R. Bowring, T. Heumuller, M. G. Christoforo and M. D. McGehee, *Energ. Environ. Sci.* **2014**, *7*, 3690-3698.
61. H. S. Kim and N. G. Park, *J. Phys. Chem. Lett.* **2014**, *5*, 2927-2934.

## Graphical Abstract



Planar heterojunction perovskite solar cells using dopant-free organic hole transport material have been developed and efficiency of 14.9% has been demonstrated.